Deep-Sea Research Part II 173 (2020) 104639

Contents lists available at ScienceDirect

Deep-Sea Research Part II

journal homepage: www.elsevier.com/locate/dsr2

Satellite estimation of carbon export by sinking particles in the California Current calibrated with sediment trap data

Mati Kahru[a,*], Ralf Goericke[a], Thomas B. Kelly[b,c], Michael R. Stukel[b,c]

[a] Scripps Institution of Oceanography, UCSD, La Jolla, CA, USA
[b] Earth, Ocean & Atmospheric Studies, Florida State University, Tallahassee, FL, USA
[c] Center for Ocean-Atmospheric Prediction Studies, Florida State University, Tallahassee, FL, USA

ARTICLE INFO

Keywords:
Export flux
Carbon export
California current ecosystem
Sinking particles
Primary production
Plankton

ABSTRACT

We evaluate a recent region-specific model of export production (Kelly et al., 2018) and some similar fits to in situ data for the California Current Ecosystem using satellite data. The model is a simple linear function of net primary productivity (NPP): Export = 0.08 × NPP + 72 where EF is export flux in mg C m^{-2} d^{-1}. We confirm that contrary to several global algorithms export efficiency (*e*-ratio = export/primary productivity) is negatively correlated with net primary productivity. We find that linear models with a steeper slope of EF relative to NPP produce better estimates of the variability range. Choice of the EF model parameterization can more than double the estimate of temporal variability (standard deviation) in satellite-derived EF time series. The best estimates of EF were obtained when using average NPP during a preceding period of ~7–8 days. This is in contrast with NPP where the best satellite estimates of in situ NPP were obtained using same day satellite data and the coefficient of determination was monotonically decreasing with increasing time lag. We also find that there is substantial unexplained variability in EF that cannot be explained by existing models.

1. Introduction

Quantification of the flux of carbon or export flux (EF, mg C m^{-2} day^{-1}) from the surface sunlit layer of the ocean to the deeper ocean is critical for predicting the atmosphere's response to climate change (Bopp et al., 2001). However, the accuracy of EF estimates is low and the current values and trends in global EF remain poorly constrained (Siegel et al., 2014). A recent study (Smith et al., 2018) of abyssal sediment fluxes at Station M in the Northeast Pacific has shown that these fluxes have become more variable during the last decade as episodic high-intensity events contribute more to the overall annual flux. This means that estimates of EF, e.g. from satellite data, need to predict not just its magnitude but also the variability range.

Models of export efficiency or e-ratio, i.e. the ratio of EF to net primary productivity (e-ratio = EF/NPP) have been developed but remain highly uncertain. Most models of e-ratio are a function of NPP but even the sign of this relationship is uncertain. While several models (e.g. Eppley and Peterson, 1979; Laws, 2004; Laws et al., 2011) assume higher export efficiency at higher productivity, other studies (Maiti et al., 2013, 2016; Stukel et al., 2013; Kelly et al., 2018, henceforth referred to as Kelly et al., 2018) have found lower export efficiency at higher productivity, i.e. a negative relationship between e-ratio and NPP. It has been hypothesized that the negative relationship between e-ratio and NPP is due to the temporal and spatial mismatch of the corresponding EF and NPP measurements. For example, it is feasible that EF on any day is not a tight function of NPP on the same day but rather a positive function of the average production over a number of days preceding the measured flux. By using daily satellite data, it is possible to estimate NPP during any day and make averages or other composites of NPP during a preceding period of any number of days. Recently, Stukel et al. (2019) assembled a multi-year dataset of EF and other variables from a set of Lagrangian sediment trap measurements conducted in the Southern California Current Ecosystem (CCE). Stukel et al. (2015) used a portion of this dataset to show that existing satellite algorithms did a poor job of reconstructing spatiotemporal variability in export efficiency in the CCE region, while Kelly et al., 2018 used part of this dataset to formulate a statistically fitted model of EF for this domain. Kelly et al., 2018 excluded stations from frontal zones and aimed at evaluating the effects of the ENSO. In this paper, we are using the extended Stukel et al. (2019) dataset to validate satellite derived EF estimates. We also evaluate if using satellite estimates of NPP during a preceding period of variable length will improve estimates of EF.

* Corresponding author.
E-mail address: mkahru@ucsd.edu (M. Kahru).

https://doi.org/10.1016/j.dsr2.2019.104639
Received 11 May 2019; Received in revised form 22 August 2019; Accepted 22 August 2019
Available online 26 August 2019

2. Methods

2.1. In situ data

The dataset for this study was derived from eight approximately month-long cruises of the CCE-LTER program (Goericke and Ohman, 2015). On these cruises, we employed a quasi-Lagrangian sampling scheme. During two-to five-day Lagrangian experiments, we followed a patch of water marked with an in situ experimental array with satellite-enabled surface float and a 3 × 1-m drogue centered at 15-m depth in the mixed layer (Landry et al., 2009). The experimental array included attachment points for mesh bags containing incubation bottles for $H^{14}CO_3^-$ uptake net primary production (NPP) measurements (Morrow et al., 2018). NPP was measured daily at six to eight depths spanning the euphotic zone. An additional, identically drogued array was deployed for the length of each Lagrangian experiment with a VERTEX-style surface-tethered sediment trap at a depth of 100 m (Knauer et al., 1979; Stukel et al., 2013). Sediment traps consisted of a cylindrical polycarbonate tube (8:1 aspect ratio, width:height) with a baffle on top consisting of smaller, beveled tubes with similar aspect ratio. Tubes were deployed with a formaldehyde brine. Upon recovery, the overlying seawater was removed from each tube, and > 200-μm swimming metazoans were removed from the sample. Tubes were then subsampled and filtered through pre-combusted filters for carbon/nitrogen or ^{234}Th analyses. For additional details, see Morrow et al. (2018). ^{238}U–^{234}Th deficiency profiles were also measured twice per cycle and used as an independent test on the accuracy of sediment traps, and found no substantial over- or under-collection of ^{234}Th (Stukel et al., 2019). We thus believe that our sediment trap results are unbiased estimates of export flux in the region. The average duration of sediment trap deployments was 3.0 days and satellite match-ups were created for the mid-point of each deployment. Vertical flux at sediment trap depths was normalized to the base of the euphotic zone (1% light level) using an exponential fit (see Kelly et al., 2018).

The eight cruises span a wide range of ecosystem states in the CCE and featured different sampling plans. The P0704 (April 2007) and P0810 (August 2010) cruises were conducted during El Niño neutral conditions and focused on sampling homogeneous water parcels (i.e. regions without strong mesoscale fronts or eddies) across a wide range of communities varying from coastal, upwelling-influenced, diatom-dominated communities to oligotrophic offshore communities dominated by picoplankton. The P1408 (August 2014) and P1604 (April 2016) cruises utilized a similar sampling plan to investigate changes in the CCE driven by the 2013–2014 North Pacific heat wave and ensuing 2015–2016 El Niño (Bond et al., 2015; Jacox et al., 2016; Kahru et al., 2018). Results from these four cruises are summarized in Kelly et al. (2018). During the P0904, P1106, and P1208 cruises (April 2009, June 2011, and August 2012, respectively), the research focus was on investigating the impact of mesoscale fronts on plankton communities and biogeochemical processes. Hence, Lagrangian studies were conducted within and to either side of distinct fronts with clearly defined sea surface temperature and sea surface chlorophyll features. Results showed that carbon export was elevated near these features, relative to what would be expected in non-frontal regions with similar NPP (Krause et al., 2015; Stukel et al., 2017a, 2017b). The P1706 (June 2017) cruise was conducted in different locations along a highly productive mesoscale filament that was transporting coastal water offshore.

2.2. Satellite data

Surface chlorophyll-a concentration (Chla, mg m^{-3}) was estimated with a regionally optimized algorithm for the California Current (Kahru et al., 2012, 2015). The algorithm calculates daily Chla estimates from remote sensing reflectance (Rrs) of multiple ocean color sensors and then merges those individual estimates into daily mapped datasets. The sensors included were SeaWiFS (2007–2009) MERIS (2007–2012), MODIS-Aqua (2007–2016), MODIS-Terra (2007–2016) and VIIRS-SNPP (2012–2016). The input datasets of Rrs were retrieved from the respective NASA (https://oceancolor.gsfc.nasa.gov) and ESA (http://merci-srv.eo.esa.int/merci/welcome.do for MERIS) websites. In this work, we used merged datasets at both 1 km and 4 km spatial resolutions (https://www.wimsoft.com/CC4km.htm).

Daily net primary production (NPP, mg C m^{-2} day^{-1}) was calculated from daily datasets of Chla, photosynthetically active radiation (PAR, einstein m^{-2} day^{-1}) and sea-surface temperature (SST, C°) using the well-known VGPM algorithm (Behrenfeld and Falkowski, 1997) as empirically modified in Kahru et al. (2009). Daily datasets of PAR (Frouin et al., 1989) from individual sensors (SeaWiFS, MODIS-Terra, MODIS-Aqua and VIIRS-SNPP) were downloaded fromhttps://oceancolor.gsfc.nasa.gov and merged. Daily SST datasets were downloaded as optimally interpolated sea-surface temperature (OISST) (Reynolds et al., 2007) from https://www.ncdc.noaa.gov/oisst.

Satellite match-ups for in situ data were found as averages of 3 × 3 pixel values centered at the nearest pixel corresponding to the position of the float at mid-time of the deployment.

As the default model to calculate EF we used the regionally fitted Kelly et al., 2018 model that is a linear function of NPP (EF = 0.08 x NPP + 72). Notably, this model was specifically designed to test the general response of the CCE to interannual variability (specifically, El Niño) and hence excluded results from front-focused cruises, which exhibited higher than typical carbon export.

2.3. Statistical analyses

Relationships between export flux and NPP were evaluated using both the ordinary least squares (OLS) linear regression and a Type II linear regression that incorporates different uncertainty estimates for each data point (York et al., 2004). We note that when the independent variable is not controlled (as in our experiments), the OLS is the most appropriate regression approach for predicting the value of a dependent variable, while the Type II regression is more appropriate for determining the relationship between the two variables. Thus, if the goal is to estimate the export flux from NPP at a single location, the OLS should be expected to give a more accurate prediction. However, it will underestimate the variability of the predicted variable, relative to the York Type II regression. As the distribution of NPP values in the CCE is close to lognormal (Kahru et al., 2009), we evaluated the goodness of satellite estimates of NPP and EF using statistics applied to log10 values. For satellite to in situ comparisons, we assumed that O_i is the ith observation of an in situ variable and P_i is the corresponding predicted satellite variable. The mean absolute percentage error (MAPE) was calculated as MAPE = 100 × mean (|(Pi − Oi)/Oi|), the median absolute percentage error (MdAPE) as MdAPE = 100 × median (|(Pi − Oi)/Oi|), the median absolute percentage error (MdAPE) as MdAPE = 100 × median ($|(P_i - O_i)/O_i|$), the median unbiased absolute percentage error (MdUAPE) as MdUAPE = 100 × median ($|(P_i - O_i)/(0.5*(P_i + O_i))|$). Mean relative percent error (MRPE) was calculated as MRPE = 100 × mean ((Pi − Oi)/Oi). Mean bias was calculated as mean (Pi − Oi).

3. Results

3.1. Match-ups with satellite data

For the total of 35 in situ cycles of EF measurements, we obtained 15 same day satellite match-ups with estimated NPP fields (Fig. 1). Most match-ups had all 9 pixels (i.e. 3 × 3) as valid while one match-up had 6 valid pixels. The availability of matching daily NPP data is controlled by the merged Chla dataset that is limited by clouds as the merged PAR and SST datasets have no missing data. By increasing the period over which match-ups are accepted, the number of match-ups

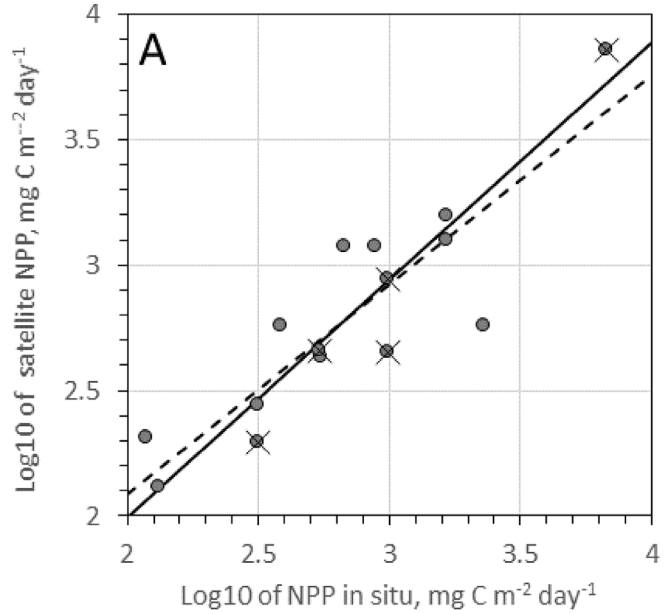

Fig. 1. Same day match-ups of satellite-derived water column productivity versus in situ measured productivity in Log10 scales. N = 15, R2 = 0.78. The crossed circles are from the "front" cruises of 2009, 2011, 2012, 2017. The dashed line is the OLS regression and the solid line is the Type II regression.

increases as longer period composites fill more of the missing pixels in daily images. For example, using a mean composite over 11 day periods preceding the in situ cycle increases the number of match-ups to 26 (out of 35). Satellite estimate of NPP for samples with same day match-ups is quite good (Fig. 1, $R^2 = 0.79$), enhanced by the wide range of measurements. A more typical R^2 value for satellite estimates of NPP (obtained for a much larger dataset) is 0.66 (Kahru et al., 2009). The highest value in the NPP match-ups is extremely high (6770 mg C m^{-2} day^{-1}) as it exceeds the highest NPP measured by the CalCOFI program (5946 mg C m^{-2} day^{-1}) since 1984. The mean and median of the NPP values measured by CalCOFI are respectively 396 and 254 mg C m^{-2} day^{-1}.

When combining all in situ data (Fig. 2, N = 35), including the "frontal" cycles, the relationship between EF and NPP becomes noisy and it is difficult to approximate the scatter with a good relationship. We compared satellite match-ups with three simple models: The Kelly et al., 2018 model (EF = 0.08 × NPP + 72 mg C m^{-2} d^{-1}), the OLS model (Fig. 2, EF = 0.07 × NPP +147 mg C m^{-2} d^{-1}) and the Type II model (Fig. 2, EF = 0.28 × NPP +10 mg C m^{-2} d^{-1}). The higher intercept in the OLS model, relative to the Kelly et al., 2018 model is likely driven by the inclusion of cruise data conducted in mesoscale fronts and filaments, which had enhanced export efficiency compared to the homogeneous water parcels investigated by Kelly et al., 2018 (Stukel et al., 2017a, 2017b).

The 15 same-day satellite match-ups shown in Fig. 1 for NPP are shown for the three versions of EF algorithms in Fig. 3. The relationships were significantly weaker, compared to satellite NPP estimates and R^2 (using log transformed export) varied from 0.22 (OLS), to 0.26 (Kelly et al., 2018) to 0.39 (Type II, Table 1). The dynamic range of the estimated EF values (excluding the single outlier point) is compressed for the OLS and Kelly et al., 2018 models (Fig. 3A and B). In contrast, the Type II regression in Fig. 3C retrieves EF values that are distributed approximately in the same range and symmetrically on either side of the one to one line as the in situ values (excluding the one extreme point). The full range of in situ EF values in the match-up dataset (N = 15) in log10 units (i.e. max – min = 1.00 for in situ data) is closest to the full range in the Kelly et al., 2018 model (Table 1). However, this agreement in total range was driven entirely by one extreme point corresponding to a coastal cycle in the P1706 'mesoscale filament' cruise that had much higher NPP than other cycles (6769 mg C m^{-2} d^{-1}), but moderate EF (399 mg C m^{-2} d^{-1}). The Type II regression overestimated the total range of the data as a direct result of this data point (Type II predicted 1998 mg C m^{-2} d^{-1} for this cycle). However, if this point is excluded, the Kelly et al., 2018 and OLS regressions both show substantially reduced variability relative to the in situ data sets, while the Type II regression matches the variability well. The Type II regression also provided improved results in many other statistics (Table 1). Furthermore, when regressing the log-transformed model predictions against the log-transformed in situ values, the Type II regression had an intercept that was closer to zero and a slope that was closer to one. It thus appeared that using a steeper slope was crucial to better predicting the full variability range, although use of this steeper k coastal blooms.

3.2. Export production as a delayed function of previous production

Previous studies have determined an inverse relationship between the *e*-ratio measured in situ and NPP in the CCE (Stukel et al., 2013; Kelly et al., 2018). A similar inverse relationship found in the Southern Ocean (Maiti et al., 2013) and in the Gulf of Mexico (Maiti et al., 2016) has been hypothesized to result from a temporal lag between production and export, obfuscating the patterns between paired near instantaneous measurements (K. Maiti, pers. comm., Laws and Maiti, 2019). To determine if such a temporal delay causes the inverse relationship found in the CCE, we created temporally averaged NPP products for each of the in situ cycles with periods from 2 to 13 days. We then found match-ups between in situ EF values and for EF calculated for average NPP during each of the preceding periods. It appears

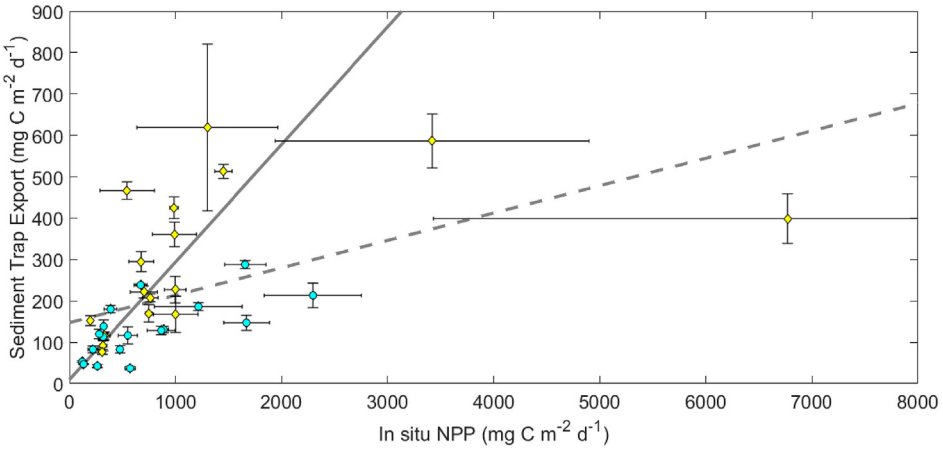

Fig. 2. Measured in situ EF at the base of the euphotic zone versus in situ productivity. Yellow diamonds are from mesoscale front and filament cruises. Cyan circles are from non-front cruises (i.e. cruises used by Kelly 2018). Dashed gray line is OLS regression (EF = 0.0662 × NPP + 147). Solid gray line is York Type II regression (EF = 0.284 × NPP + 9.75). N = 35.

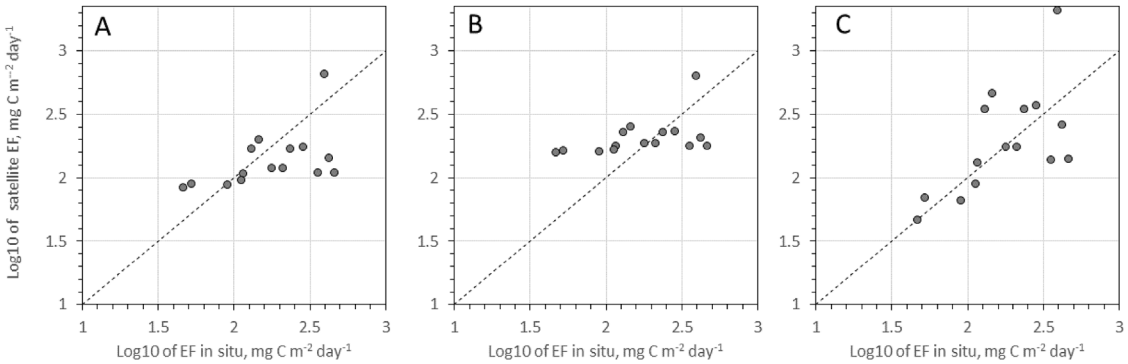

Fig. 3. Satellite estimates of EF with same-day match-ups using (A) Kelly et al. (2018); (B) OLS regression from Fig. 2; and (C) the York Type II model in Fig. 2. The dotted line is the one to one line.

Table 1
Comparison of different statistics of satellite EF retrievals using the Kelly et al., (2018) model, OLS and York Type II regressions in Fig. 1B. Bold values show improved estimates. The log10 range of in situ data was 1.00.

Statistic using log10 values	EF calculated as Kelly et al., (2018)	OLS, Fig. 1B, EF = 0.066 × NPP +147	York, Fig. 1B, EF = 0.284 × NPP +9.8
Range (max – min)	**0.90**	0.60	1.65
Mean absolute percent error (MAPE)	**10.02**	11.02	10.13
Median absolute percent error (MdAPE)	8.12	10.70	**6.71**
Mean unbiased absolute percent error (MUAPE)	10.47	10.53	**9.91**
Median unbiased absolute percent error (MdUAPE)	8.46	10.16	**6.49**
Mean relative percent error (MRPE)	−3.84	4.68	**1.82**
Median relative percent error (MdRPE)	−3.95	7.46	**−0.30**
Mean bias	−0.11	0.07	**0.03**
Intercept of OLS regression	1.32	1.81	**0.42**
Slope of OLS regression	0.36	0.22	**0.83**
Coefficient of determination (R^2)	0.26	0.22	**0.39**

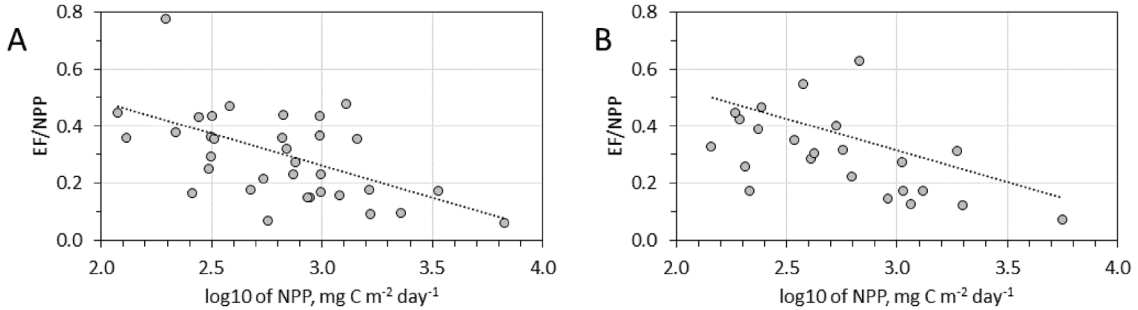

Fig. 4. *e*-ratio (EF/NPP) versus log10 of NPP. (A), using in situ EF and in situ NPP; (B) using in situ EF and satellite estimated average 6-day NPP prior to EF measurement. The dotted lines are the OLS linear regressions: (A) *e*-ratio = 0.93–0.223 × log10NPP and (B) *e*-ratio = 0.98–0.220 × log10NPP.

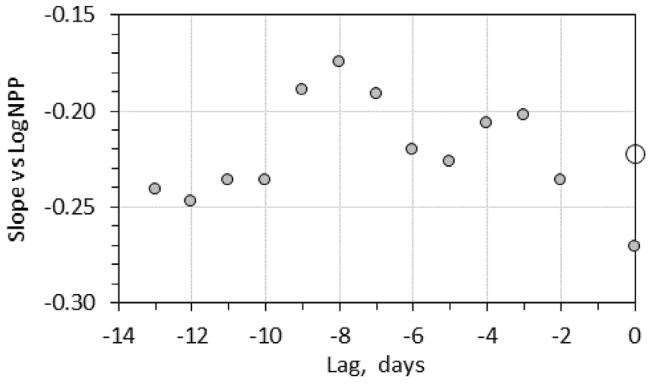

Fig. 5. Linear slope of the *e*-ratio versus log10 of NPP (see Fig. 3) estimated for preceding periods of variable length (corresponding to the lag) and for the in situ data (large open circle).

that using the average production during the preceding 2–13 days does not change the generally negative relationship between NPP and the *e*-ratio (Figs. 4 and 5). In fact, the negative relationship expressed as the slope of *e*-ratio versus $\log_{10}$(NPP) does not seem to depend on using average NPP during any of the preceding periods and is no different from the slope for in situ data (Fig. 5. The relationships in Figs. 4 and 5 were calculated using the Type II model but the same conclusions could be reached when using the Kelly et al., 2018 model.

The effect of using average NPP estimates during preceding days compared to those of the same day was investigated by comparing temporally-averaged satellite NPP (or EF determined from temporally-averaged NPP) to instantaneous in situ measurements. NPP estimates are most accurate using the same day satellite data and the coefficient of determination decreases with longer periods of temporal averaging prior to the in situ measurement (Fig. 6). This pattern reflects the combination of short-term (e.g. changes in cloud cover) and longer-term (e.g. changes in phytoplankton biomass and community composition) drivers of variability in NPP as well as the effect of advection on the spatial accuracy of satellite match-ups. In contrast, the pattern is

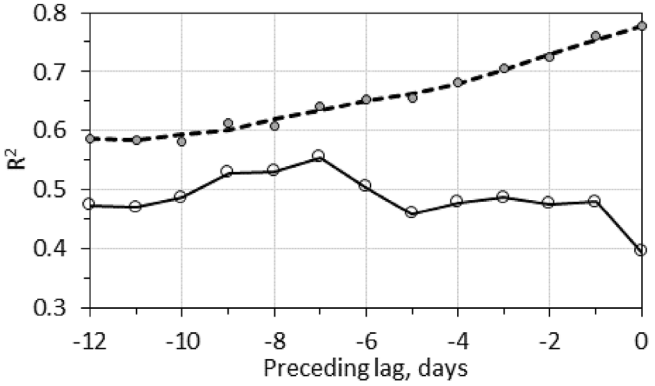

Fig. 6. Coefficient of determination (R^2) between in situ measurements and satellite estimates averaged during a preceding period of a number of days as a function the respective preceding period of averaging for NPP (gray filled circles, the dashed line has been smoothed with a 3-point smoothing boxcar filter) and EF (open circles connected with a solid line).

quite different for estimating EF. The highest coefficient of determination between satellite estimated EF and in situ EF is not when using same day satellite data but when using average NPP during a preceding period of 7–8 days. The differences between R^2 of match-ups with different preceding periods are relatively small and statistically not significant due to the small number of match-ups (increasing from 15 at same day to 23 at 3 days and to 27 at 7 days). However, the lack of decrease in R^2 with increasing time lag is obvious and the differences between the responses of estimating NPP and estimating EF on the time lag may indeed indicate that the sinking flux out of the euphotic zone depends on production during the previous 7–8 days.

3.3. Effects of the EF model on the time series of EF at station M

To evaluate the differences resulting from using different EF models on satellite-derived time series we chose an area around Station M (34°50′N, 123°0′ W) in a transition region between coastal upwelling areas of the CCE and the oligotrophic offshore domain. Observations at Station M have been carried out since 1989 (Smith et al., 2013, 2018). We used a time series of NPP calculated at 5-day intervals using 4-km satellite data (http://www.wimsoft.com/CC4km.htm) and applied both the Kelly et al., 2018 model and the Type II model. The valid EF pixel values were averaged in a circle with 100-km radius. The parameterization of the EF model has a dramatic effect on estimated EF time series (Fig. 7), particularly on estimates of EF variability. For example, standard deviation (SD) of the time series of EF for the period of 2007–2018 more than doubled from 24.2 mg C m^{-2} day^{-1} (0.078 in log_{10} units) when using the Kelly et al., 2018 model to 65.8 (0.185 in log_{10} units) mg C m^{-2} day^{-1} when using the Type II model. As shown by Smith et al. (2018), episodic fluxes play an increasing role in the total flux reaching the bottom. It is therefore important to investigate the processes driving variability in EF for the in situ data (see discussion), as well as the differences between two algorithms derived from a similar dataset. We note that the use of the OLS regression in Kelly et al., 2018 was chosen to minimize the error between predictions and in situ data at any specific location and time. However, the OLS (which essentially is a mean-reverting regression), by definition underestimates the slope of the underlying relationships between two uncontrolled variables (e.g. NPP and EF). The Type II model thus may give a better estimate of the true variability in EF, which could be important for estimating important episodic energy pulses to benthic communities.

Another obvious feature of the time series is the suppression of both the magnitude and the variability of EF during the 2015 Northeast Pacific warming event (Jacox et al., 2016), regardless of which algorithm is used. This suppressed EF was related to a decrease in Chla, NPP, and frequency of fronts throughout our study region (Kahru et al., 2018; Kelly et al., 2018). Notably, decreased carbon flux into near-bottom sediment traps at Station M was also measured during this time period (Smith et al., 2018).

4. Discussion

Using a 29-year record of in situ observations at Station M (NE Pacific, 4000-m depth) Smith et al. (2018) showed that episodic peaks in sedimenting fluxes play an increasingly important role for the deep communities. According to in situ measurements the contribution of high-magnitude episodic events has increased from an average of 19% for the entire data set (1989–2017) to 43% in the most recent years (2011–2017). The Kelly et al., 2018 model was used in Smith et al. (2018) to evaluate linkages between surface conditions estimated from satellite data and the deep water in situ measurements. Smith et al. (2018) found that the background (non-episodic) flux to the abyss could be well estimated by extrapolating surface flux estimated with the Kelly et al., 2018 downward using a power law model. However, this approach underestimated the episodic high flux events by ~80%. We have shown here that a portion of this underestimation is due to parameterization of the EF model using an OLS regression, which is well-suited to estimating average conditions but can have a dramatic effect on the dynamic range and variability of estimated EF. Use of a Type II regression led to more than a doubling in temporal variability of predicted flux at Station M. The satellite-derived time series using this regression (Fig. 7) shows the dramatic effects of climate variability as the 2015 North-East Pacific warming event and the 2016 El Niño severely suppressed both EF magnitude and its temporal variability. The 2015–2016 warm event was also a period of suppressed frequency of oceanic fronts (Kahru et al., 2018) that may have further reduced the part of export flux caused by subduction as subduction at fronts makes a significant addition to EF in addition to gravitational sinking (Stukel et al., 2017a, 2017b).

Use of a Type II regression only explains a portion of the variability in abyssal carbon flux noted by Smith et al. (2018). This is not surprising, because NPP alone only explains a portion of the variability in export flux seen in Fig. 2. Indeed, the highest flux events recorded in this study occurred at intermediate values of NPP. These spikes of EF are likely related to a suite of physical, biogeochemical, and ecological dynamics that affect pelagic ecosystems, only some of which are likely

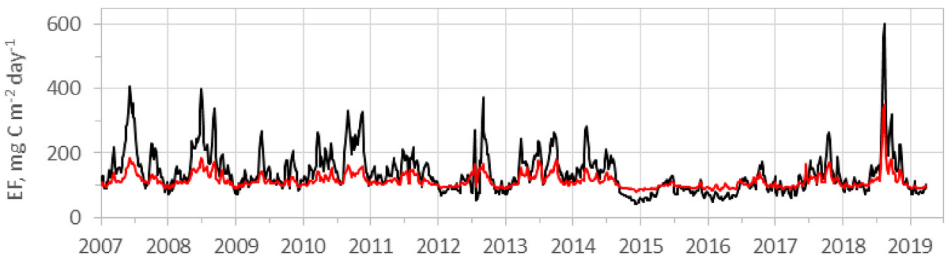

Fig. 7. Time series of satellite estimates of EF within a circle (radius = 100 km) around Station M (see Smith et al., 2018]) determined with the Kelly2018 model (red line) and the York Type II model (black line).

to be observable remotely. Stukel et al. (2017a, 2017b) and Krause et al. (2015) found enhanced fluxes associated with mesoscale fronts in the CCE. Similar impacts of mesoscale features have been found in other regions as well (Benitez-Nelson and McGillicuddy, 2008; Stemmann et al., 2008; Estapa et al., 2015). Such features are observable by satellite and may be increasing in frequency in the CCE (Kahru et al., 2012), suggesting that future studies might benefit from including presence of fronts as an explicit variable used to enhance prediction of export flux. Phytoplankton physiological changes (increased silicification resulting from Fe stress) have also been identified as processes that increase the efficiency of the biological pump in the CCE (Brzezinski et al., 2015). Although Fe stress cannot currently be detected remotely, Fe stress affects the fluorescence dynamics of phytoplankton (Kudela et al., 2006), suggesting that it can feasibly be diagnosed using autonomous floats and/or next-generation satellite sensors.

Compared to the above processes, obtaining remote information about the impact of epipelagic and mesopelagic zooplankton communities on carbon flux remains a daunting task. The specific composition of zooplankton communities can have a strong impact on carbon flux. Indeed, some of the highest magnitude episodic fluxes in the Smith et al. (2018) data set were associated with blooms of salps and the subsequent flux of their fecal pellets and carcasses to the benthos (Smith et al., 2014). Further to the north, flux to the benthos has been linked to the abundance of giant appendicularians (Robison et al., 2005), while throughout our study region fecal pellets (primarily of crustacean origin) are likely the dominant contributor to carbon flux from the euphotic zone (Morrow et al., 2018). In other regions, krill, pteropods, and salps have been identified as important producers of sinking carbon (Pfannkuche and Lochte, 1993; Manno et al., 2009; Phillips et al., 2009; Gleiber et al., 2012), while even the “mini-pellets” of protists can contribute substantially to flux (Gowing and Silver, 1985; Lampitt et al., 2009). Meanwhile, dynamic mesopelagic communities can substantially modify this downward flux. Flux-feeding zooplankton, including pteropods, phaeodarians, copepods, and polychaetes, feed efficiently on rapidly-sinking particles and can have highly variable abundances (Jackson et al., 1993; Kosobokova et al., 2002; Stukel et al., 2018; Christiansen et al., 2018). Patchy distributions of filter-feeding zooplankton, such as krill and pyrosomes, can also lead to near complete consumption of slowly-sinking particles in the shallow twilight zone (Décima et al., 2019). Incorporating the variable impact of these communities on carbon flux to the benthos may require coupling statistical or dynamical models to remotely observed NPP and other parameters.

5. Conclusions

Our results improve satellite-derived estimates of the export flux of carbon, a variable that is crucial in climate change research. They also highlight the large uncertainties that are evident in these estimates. More research using process-oriented studies is clearly needed to explain the high residual variability in modeling *e*-ratio and export fluxes. It is likely that additional sources of information must be considered to increase the accuracy of carbon flux estimates. Such data include potentially observable proxies for phytoplankton physiological status and mesoscale dynamics associated with fronts and eddies, as well as estimates of the role of zooplankton communities in particle creation and flux attenuation, which may require the use of statistical or dynamical population models.

Acknowledgments

This work was funded by NSF grants to the CCE LTER program: OCE-0417616, OCE-1026607, OCE-1637632 and OCE-1614359. MK was also funded by the David and Lucile Packard Foundation through the Monterey Bay Aquarium Research Institute. Satellite data were provided by the NASA Ocean Color Processing Group and ESA MERIS team.

Appendix A. Supplementary data

Supplementary data to this article can be found online at https://doi.org/10.1016/j.dsr2.2019.104639.

References

Behrenfeld, M.J., Falkowski, P.G., 1997. Photosynthetic rates derived from satellite based chlorophyll concentration. Limnol. Oceanogr. 42, 1–20. https://doi.org/10.4319/lo.1997.42.1.0001.

Benitez-Nelson, C.R., Mcgillicuddy Jr., D.J., 2008. Mesoscale physical–biological–biogeochemical linkages in the open ocean: an introduction to the results of the E-Flux and EDDIES programs. Deep Sea Res. Part II Top. Stud. Oceanogr. 55, 1133–1138.

Bond, N.A., Cronin, M.F., Freeland, H., Mantua, N., 2015. Causes and impacts of the 2014 warm anomaly in the NE Pacific. Geophys. Res. Lett. 42, 3414–3420. https://doi.org/10.1002/2015GL063306.

Bopp, L., Monfray, P., P., Aumont, O., Dufresne, J.-L., Le Treut, H., Madec, G., Terray, L., Orr, J.C., 2001. Potential impact of climate change on marine export production. Glob. Biogeochem. Cycles 15, 81–99. https://doi.org/10.1029/1999GB001256.

Brzezinski, M.A., Krause, J.W., Bundy, R.M., Barbeau, K.A., Franks, P., Goericke, R., Landry, M.R., Stukel, M.R., 2015. Enhanced silica ballasting from iron stress sustains carbon export in a frontal zone within the California Current. J. Geophys. Res.: Oceans 120, 4654–4669.

Christiansen, S., Hoving, H.-J., Schütte, F., Hauss, H., Karstensen, J., Körtzinger, A., Schröder, S.-M., Stemmann, L., Christiansen, B., Picheral, M., Brandt, P., Robison, B., Koch, R., Kiko, R., 2018. Particulate matter flux interception in oceanic mesoscale eddies by the polychaete *Poeobius* sp. Limnol. Oceanogr. 63, 2093–2109.

Décima, M., Stukel, M.R., López-López, L., Landry, M.R., 2019. The unique ecological role of pyrosomes in the Eastern Tropical Pacific. Limnol. Oceanogr. 64, 728–743.

Eppley, R.W., Peterson, B.J., 1979. Particulate organic matter flux and planktonic new production in the deep ocean. Nature 282, 677–680. https://doi.org/10.1038/282677a0.

Estapa, M.L., Siegel, D.A., Buesseler, K.O., Stanley, R.H.R., Lomas, M.W., Nelson, N.B., 2015. Decoupling of net community and export production on submesoscales. Glob. Biogeochem. Cycles 29, 1266–1282.

Frouin, R., Ligner, D.W., Gautier, C., 1989. A simple analytical formula to compute clear sky total and photosynthetically available solar irradiance at the ocean surface. J. Geophys. Res. 94, 9731–9742.

Gleiber, M.R., Steinberg, D.K., Ducklow, H.W., 2012. Time series of vertical flux of zooplankton fecal pellets on the continental shelf of the western Antarctic Peninsula. Mar. Ecol.: Prog. Ser. 471, 23–36.

Goericke, R., Ohman, M.D., 2015. Introduction to CCE-LTER: responses of the California current ecosystem to climate forcing. Deep Sea Res. Part II Top. Stud. Oceanogr. 112, 1–5. https://doi.org/10.1016/j.dsr2.2014.12.001.

Gowing, M.M., Silver, M.W., 1985. Minipellets - a new and abundant size class of marine fecal pellets. J. Mar. Res. 43, 395–418.

Jackson, G.A., Najjar, R.G., Toggweiler, J.R., 1993. Flux feeding as a mechanism for zooplankton grazing and its implications for vertical particulate flux. Limnol. Oceanogr. 38, 1328–1331.

Jacox, M.G., Hazen, E.L., Zaba, K.D., Rudnick, D.L., Edwards, C.A., Moore, A.M., Bograd, S.J., 2016. Impacts of the 2015–2016 El Niño on the California current system: early assessment and comparison to past events. Geophys. Res. Lett. 43, 7072–7080. https://doi.org/10.1002/2016GL069716.

Kahru, M., Kudela, R., Manzano-Sarabia, M., Mitchell, B.G., 2009. Trends in primary production in the California Current detected with satellite data. J. Geophys. Res. Ocean. 114, 1–7. https://doi.org/10.1029/2008JC004979.

Kahru, M., Kudela, R.M., Manzano-Sarabia, M., Greg Mitchell, B., 2012. Trends in the surface chlorophyll of the California Current: merging data from multiple ocean color satellites. Deep. Res. Part II Top. Stud. Oceanogr 77–80, 89–98. https://doi.org/10.1016/j.dsr2.2012.04.007.

Kahru, M., Kudela, R.M., Anderson, C.R., Mitchell, B.G., 2015. Optimized merger of ocean chlorophyll algorithms of MODIS-Aqua and VIIRS. IEEE Geosci. Remote Sens. Lett. 12, 2282–2285. https://doi.org/10.1109/LGRS.2015.2470250.

Kahru, M., Jacox, M.G., Ohman, M.D., 2018. CCE1: decrease in the frequency of oceanic fronts and surface chlorophyll concentration in the California Current System during the 2014–2016 northeast Pacific warm anomalies. Deep-Sea Res. Part I Oceanogr. Res. Pap. https://doi.org/10.1016/j.dsr.2018.04.007.

Kelly, T.B., Goericke, R., Kahru, M., Song, H., Stukel, M., 2018. Cce II: spatial and interannual variability in export efficiency and the biological pump in an eastern boundary current upwelling system with substantial lateral advection. Deep-Sea Res. I 140, 14–25. https://doi.org/10.1016/j.dsr.2018.08.007.

Knauer, G.A., Martin, J.H., Bruland, K.W., 1979. Fluxes of particulate carbon, nitrogen, and phosphorus in the upper water column of the northeast Pacific. Deep Sea Res. Part A, Oceanogr. Res. Pap. 26, 97–108. https://doi.org/10.1016/0198-0149(79)90089-X.

Kosobokova, K., Hirche, H.-J., Scherzinger, T., 2002. Feeding ecology of Spinocalanus antarcticus, a mesopelagic copepod with a looped gut. Mar. Biol. 141, 503–511.

Krause, J.W., Brzezinski, M.A., Goericke, R., Landry, M.R., Ohman, M.D., Stukel, M.R., Taylor, A.G., 2015. Variability in diatom contributions to biomass, organic matter production and export across a frontal gradient in the California Current Ecosystem. J. Geophys. Res. Ocean. 120, 1032–1047. https://doi.org/10.1002/2014JC010472.

Kudela, R., Garfield, N., Bruland, K., 2006. Bio-optical signatures and biogeochemistry from intense upwelling and relaxation in coastal California. Deep-Sea Res. Part II 53, 2999–3022.

Lampitt, R., Salter, I., Johns, D., 2009. Radiolaria: major exporters of organic carbon to the deep ocean. Glob. Biogeochem. Cycles 23, GB1010. https://doi.org/10.1029/2008GB003221.

Landry, M.R., Ohman, M.D., Goericke, R., Stukel, M.R., Tsyrklevich, K., 2009. Lagrangian studies of phytoplankton growth and grazing relationships in a coastal upwelling ecosystem off Southern California. Prog. Oceanogr. 83, 208–216. https://doi.org/10.1016/j.pocean.2009.07.026.

Laws, E., 2004. Export flux and stability as regulators of community composition in pelagic marine biological communities: implications for regime shifts. Prog. Oceanogr. 60, 343–354. https://doi.org/10.1016/j.pocean.2004.02.015.

Laws, E.A., Maiti, K., 2019. The relationship between primary production and export production in the ocean: effects of time lags and temporal variability. Deep-Sea Res. Part I Oceanogr. Res. Pap. 148, 100–107. https://doi.org/10.1016/j.dsr.2019.05.006.

Laws, E.A., D'Sa, E., Naik, P., 2011. Simple equations to estimate ratios of new or export production to total production from satellite-derived estimates of sea surface temperature and primary production. Limnol Oceanogr. Methods 9, 593–601. https://doi.org/10.4319/lom.2011.9.593.

Maiti, K., Charette, M.A., Buesseler, K.O., Kahru, M., 2013. An inverse relationship between production and export efficiency in the Southern Ocean. Geophys. Res. Lett. 40, 1557–1561. https://doi.org/10.1002/grl.50219.

Maiti, K., Bosu, S., D'Sa, E.J., Adhikari, P.L., Sutor, M., Longnecker, K., 2016. Export fluxes in northern Gulf of Mexico - comparative evaluation of direct, indirect and satellite-based estimates. Mar. Chem. 184, 60–77. https://doi.org/10.1016/j.marchem.2016.06.001.

Manno, C., Tirelli, V., Accornero, A., Fonda Umani, S., 2009. Importance of the contribution of *Limacina helicina* faecal pellets to the carbon pump in Terra Nova Bay (Antarctica). J. Plankton Res. 32, 145–152.

Morrow, R., Goericke, R., Kelly, T.B., Landry, M.R., Ohman, M.D., Stephens, B.M., Stukel, M.R., 2018. Primary productivity, mesozooplankton grazing, and the biological pump in the California Current Ecosystem: variability and response to El Niño. Deep. Res. I 140, 52–62. https://doi.org/10.1016/j.dsr.2018.07.012.

Pfannkuche, O., Lochte, K., 1993. Open ocean pelago-benthic coupling: cyanobacteria as tracers of sedimenting salp feces. Deep-Sea Res. I 40, 727–737.

Phillips, B., Kremer, P., Madin, L.P., 2009. Defecation by *Salpa thompsoni* and its contribution to vertical flux in the Southern Ocean. Mar. Biol. (Berl.) 156, 455–467.

Reynolds, R.W., Smith, T.M., Liu, C., Chelton, D.B., Casey, K.S., Schlax, G., 2007. Daily high-resolution blended analyses for sea surface temperature. J. Clim. 20, 5473–5496. https://doi.org/10.1175/2007JCLI1824.1.

Robison, B.H., Reisenbichler, K.R., Sherlock, R.E., 2005. Giant larvacean houses: rapid carbon transport to the deep sea floor. Science 308, 1609–1611.

Siegel, D.A., Buesseler, K.O., Doney, S.C., Sailley, S.F., Behrenfeld, M.J., Boyd, P.W., 2014. Global assessment of ocean carbon export by combining satellite observations and food-web models. Glob. Biogeochem. Cycles 28, 181–196. https://doi.org/10.1002/2013GB004743.Received.

Smith, K.L., Ruhl, H.A., Kahru, Huffard, C.L., Sherman, A.D., 2013. Deep ocean communities impacted by changing climate over 24 years in the abyssal northeast Pacific Ocean. Proc. Natl. Acad. Sci. 110 (49), 19838–19841.

Smith Jr., K.L., Sherman, A.D., Huffard, C.L., Mcgill, P.R., Henthorn, R., Von Thun, S., Ruhl, H.A., Kahru, M., Ohman, M.D., 2014. Large salp bloom export from the upper ocean and benthic community response in the abyssal northeast Pacific: day to week resolution. Limnol. Oceanogr. 59, 745–757.

Smith Jr., K.L., Ruhl, H.A., Huffard, C.L., Messie, M., Kahru, M., 2018. Episodic organic carbon fluxes from surface ocean to abyssal depths during long-term monitoring in NE Pacific. Proc. Natl. Acad. Sci. www.pnas.org/cgi/doi/10.1073/pnas.1814559115.

Stemmann, L., Prieur, L., Legendre, L., Taupier-Letage, I., Picheral, M., Guidi, L., Gorsky, G., 2008. Effects of frontal processes on marine aggregate dynamics and fluxes: an interannual study in a permanent geostrophic front (NW Mediterranean). J. Mar. Syst. 70, 1–20.

Stukel, M.R., Ohman, M.D., Benitez-Nelson, C.R., Landry, M.R., 2013. Contributions of mesozooplankton to vertical carbon export in a coastal upwelling system. Mar. Ecol. Prog. Ser. 491, 47–65. https://doi.org/10.3354/meps10453.

Stukel, M.R., Kahru, M., Benitez-Nelson, C.R., Décima, M., Goericke, R., Landry, M.R., Ohman, M.D., 2015. Using Lagrangian-based process studies to test satellite algorithms of vertical carbon flux in the eastern North Pacific Ocean. J. Geophys. Res. Ocean. 120, 7208–7222. https://doi.org/10.1002/2015JC011264.

Stukel, M.R., Aluwihare, L.I., Barbeau, K.A., Chekalyuk, A.M., Goericke, R., Miller, A.J., Ohman, M.D., Ruacho, A., Song, H., Stephens, B.M., Landry, M.R., 2017a. Mesoscale ocean fronts enhance carbon export due to gravitational sinking and subduction. Proc. Natl. Acad. Sci. 114, 1252–1257. https://doi.org/10.1073/pnas.1609435114.

Stukel, M.R., Song, H., Goericke, R., Miller, A.J., 2017b. The role of subduction and gravitational sinking in particle export, carbon sequestration, and the remineralization length scale in the California Current Ecosystem. Limnol. Oceanogr. https://doi.org/10.1002/lno.10636.

Stukel, M.R., Biard, T., Krause, J.W., Ohman, M.D., 2018. Large phaeodaria in the twilight zone: their role in the carbon cycle. Limnol. Oceanogr. 63, 2579–2594.

Stukel, M.R., Kelly, T.B., Aluwihare, L.I., Barbeau, K.A., Goericke, R., Krause, J.W., Landry, M.R., Ohman, M.D., 2019. The Carbon:234Thorium ratios of sinking particles in the California Current Ecosystem 1: relationships with plankton ecosystem dynamics. Mar. Chem. 211, 37–51.

York, D., Evensen, N.M., Martinez, M.L., Delgado, J.D., 2004. Unified equations for the slope, intercept, and standard errors of the best straight line. Am. J. Phys. 72, 367–375.